Ecological Indicators 84 (2018) 811–819

Contents lists available at ScienceDirect

Ecological Indicators

journal homepage: www.elsevier.com/locate/ecolind

Research paper

Evaluation of agricultural water demand under future climate change scenarios in the Loess Plateau of Northern Shaanxi, China

Sun S.K.[a,b,c,1], Li C.[a,b,1], Wu P.T.[b,c,*], Zhao X.N.[a,b,c,*], Wang Y.B.[a,b,c]

[a] College of Water Resources and Architectural Engineering, Northwest A & F University, Yangling 712100, China
[b] Key Laboratory of Agricultural Soil and Water Engineering in Arid and Semiarid Areas, Ministry of Education, Northwest A & F University, Yangling 712100, Shaanxi, China
[c] Institute of Water Saving Agriculture in Arid regions of China, Northwest A & F University, Yangling 712100, Shaanxi, China

ARTICLE INFO

Keywords:
Climate change
Agricultural water use
Evapotranspiration
Irrigation water requirement

ABSTRACT

Climate change will affect the future availability of water resources for agriculture. An understanding of the impact of future climate change on regional agricultural water use can provide a basis for regional agricultural production and water management. This paper evaluated the agricultural water demand under three future climate change scenarios in the Loess Plateau of northern Shaanxi (LPNS), China. The results showed that in the scenarios RCP2.6, RCP4.5, and RCP8.5, the temperature, effective precipitation, and relative humidity were on the rise, the wind speed decreased slightly, and the trend of sunshine duration was unclear. The irrigation water requirements of the main crops exhibited a downward trend under future climate change scenarios. The decreasing trend of the irrigation water requirement was highest in the RCP8.5 (−0.90%) scenario, followed by the RCP4.5 (−0.77%/year) and the RCP2.6 (−0.30%/year) scenarios. Based on the impact of the changes in the evapotranspiration of future crops and the effective precipitation in the RCP2.6 scenario, the irrigation water requirements of the agricultural industry showed a downward trend and decreased from 1.84×10^9 m^3/year (2010–2014 average) to 1.29×10^9 m^3/year (2040–2049 average); the irrigation water requirements of the agricultural industry showed a significant downward trend ($P < 0.05$) in the RCP4.5 and RCP8.5 scenarios, decreasing from 1.84×10^9 m^3/year (2010–2014 average) to 1.20×10^9 m^3/year (2040–2049 average) and 1.15×10^9 m^3/year (2040–2049 average), respectively. Future research should be aimed at improving the regional climate downscaling and developing a better understanding of the responses of agriculture to regional climate change.

1. Introduction

Global warming has become an accepted fact in recent years and climate change is one of the pressing issues. Due to the increase in global temperatures, the water holding capacity and the water vapor transport of the atmosphere have increased (Menzel and Bürger, 2002; Sun et al., 2013). The imbalance between water availability and water demand causes water scarcity, which has become one of the most pressing issues in the world (Sun et al., 2016a). In many parts of the world, the hydrologic cycle has accelerated due to changes in soil moisture, runoff, and precipitation over the past century (Groisman et al., 1999; Ziegler et al., 2003; Huntington, 2006; Gao et al., 2006; Zhang et al., 2009). The Intergovernmental Panel on Climate Change (IPCC) and the Food and Agriculture Organization (FAO) of the United Nations has listed agriculture as one of the most vulnerable industries affected by climate change, particularly in developing countries. Currently, irrigation remains an important means of ensuring sufficient food production. In developing countries, the crop yields in irrigated farmland account for 60% of the total crop production (Fischer et al., 2007). Increasing competition for water between agricultural and other sectors, as well as challenges brought by climate change, future available water resources for agriculture production will continue to decline (Sun et al., 2016b).

To date, the prediction of future climate change has been mainly based on General Circulation Models (GCMs). Scientists around the world have established a series of GCMs over the past 20 years. GCMs can simulate large-scale average features well. Although the models cannot predict the future climate, they can describe the possible

* Corresponding authors at: Key Laboratory of Agricultural Soil and Water Engineering in Arid and Semiarid Areas, Ministry of Education, Northwest A & F University, Yangling 712100, Shaanxi, China.
E-mail addresses: gjzwpt@vip.sina.com (P.T. Wu), xiningz@aliyun.com (X.N. Zhao).
[1] These authors contributed equally to this work.

http://dx.doi.org/10.1016/j.ecolind.2017.09.048
Received 7 June 2017; Received in revised form 11 August 2017; Accepted 27 September 2017
Available online 05 October 2017
1470-160X/ © 2017 Published by Elsevier Ltd.

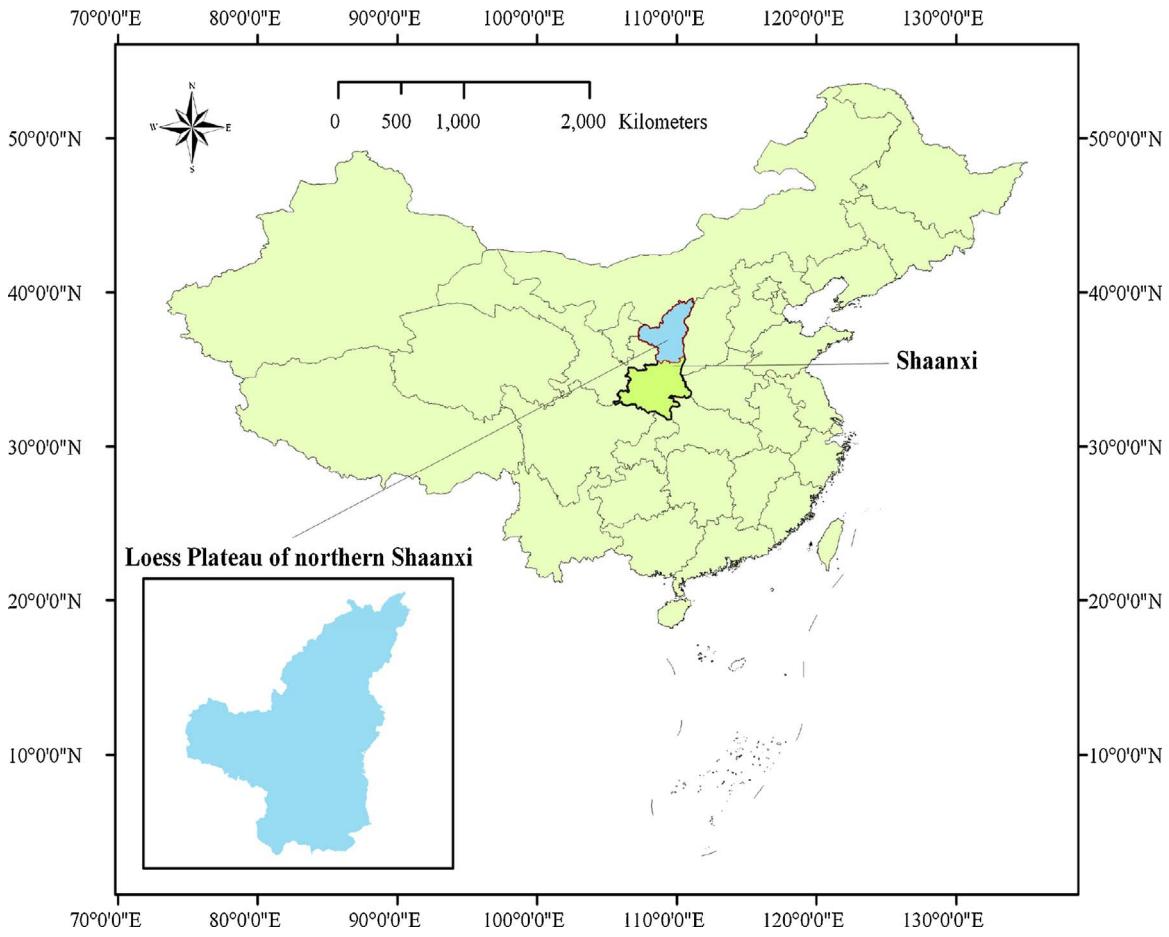

Fig. 1. The geographical location of the LPNS.

changes in the future climate. GCMs can reflect future climate change coupled with crop models that reflect crop growth changes (i.e., model simulations); this approach has been used to research the impact of climate change on irrigation water requirements, which recently has received increasing attention. Tao et al. (2003) obtained the temporal and spatial variations of reference crop evapotranspiration (ET_0), the evapotranspiration (ET_c), the soil water deficit, and the irrigation water requirements based on the Hadley Centre Coupled Model (HadCM2)-driven crop-soil-water simulation model. Silva et al. (2007) used the HadCM3 A2 and B2 scenarios combined with the crop model CROPWAT to predict the effects of climate change on rice irrigation water requirements in Sri Lanka. Tao et al. (2008) coupled the GCMs and the CERES-Rice crop models to study the relationship between global warming, rice production, and irrigation water requirements in China, and presented a probabilistic assessment of the changes in future rice production and irrigation water requirements. Moriondo and Bindi (2006) evaluated the performance of a general circulation model, a regional circulation model, and an artificial neural network for a cropping systems simulation for the present climate. Toews and Allen (2009) predicted the sensitivity of recharge to different climate models in an irrigated agricultural region by using climate change scenarios from three global climate models. Based on the Conformal Cubic Atmospheric Model driven by four GCMs, the effects of increased temperature on the initiation and the duration of key crop phenophases and on the occurrence of heat stress and cold shocks during the growing season were evaluated (Luo et al., 2014). The future distributions of *Gossypium* (cotton) and *Triticum aestivum* L. (wheat) were modeled using the CLIMEX software with the A2 emission scenario generated by the CSIRO-Mk3·0 and the MIROC-H global climate models (Shabani and Kotey, 2016). The effect of sampling weather data was evaluated for simulating the yields of winter wheat in a region in Germany over a 30-year period (1982–2011) using 12 process-based crop models (Bussel et al., 2016). Many of the previous studies have directly calculated the irrigation water requirements while ignoring the changes in rainfall patterns. Changes in irrigation water requirements are a common result of changes in crop water demand and rainfall and changes in crop water demand alone are not enough to provide a basis for the development of irrigation strategies to address climate change. Ecological fragility and a shortage of water resources are pressing issues in the Loess Plateau of northern Shaanxi (LPNS). An analysis of the supply and demand of agricultural water resources in the future and a clarification of the impact of future climate change on regional agricultural water use can provide policy support for the maintenance of regional water resources and for sustainable agricultural development.

This study aimed to explore the changes in agricultural water demand in the future by using a statistical downscaling method. First, the major climatic factors were simulated using a back propagation artificial neural network. Second, the changes in the evapotranspiration of major crops as a result of future climate change were analyzed. Finally, the characteristics of agricultural water demand were assessed by analyzing the crop evapotranspiration and effective precipitation under future climate change scenarios. The results of this study will provide a basis for understanding the potential impacts of climate change on the regional agricultural water demand and its characteristics.

2. Material and methods

2.1. Study area

The LPNS is located in the central part of the Loess Plateau in China,

and it is within the transition zone between the eastern monsoon humid region and the inland arid region. The terrain consists of high elevations in the northwest and low elevations in the southeast. The LPNS is located within 35°21′–39°34′ N and 107°28′–110°31′ E (Wu et al., 2014; Li et al., 2017). It comprises an area of 80,607 km^2, has an annual daily mean temperature in the range of 6–11 °C, an annual precipitation of 400–600 mm, and an annual sunshine duration of 2300–2914 h. The study area includes the counties of Luochuan, Yanan, Suide, Hengshan, Wuqi, Yulin, Dingbian, Yanchang, Jingbian, and Shenmu (Fig. 1).

2.2. Material

2.2.1. Meteorological data

The meteorological data used in this study were collected from 1960 to 2014 in LPNS, including wind speed (m/s), sunshine duration (h), daily mean temperature (°C), daily maximum temperature (°C), daily minimum temperature (°C), relative humidity (%), and precipitation (mm). The climatic data were provided by the China Meteorological Administration (CMA, 2015). Geographic information, such as latitude, longitude, and altitude of the aforementioned ten sites in the Shaanxi Province was also obtained.

2.2.2. General circulation model data

The general circulation model data used in this study were collected from 1960 to 2040 in the LPNS, including wind data, temperature, heat flux, etc. The general circulation model data were provided by the Canadian Centre for Climate Modelling and Analysis (CCCma, 2017). The CanESM2 model is currently extensively used and a substantial amount of research demonstrates that the model has excellent applicability for the research of the China region. For example, using the CanESM2 model, Wen et al. (2013) studied model-simulated patterns of changes in extreme temperatures in China during the period of 1961–2007 using an optimal detection method. Sun et al. (2015) used CanESM2 model data from the period of 1996–2005 to downscale in China. Results showed that the simulated meteorological factor was greater than 56.4% of the sites with a correlation coefficient greater than 0.98. The correlation coefficient was below 0.92 for 1.2% of the sites. The mean relative error was less than 0.2 and greater than 0.6 for 82.9% and 1.1% of the sites, respectively. Therefore, this study used the three climate scenarios RCP2.6, RCP4.5, and RCP8.5 of the CanESM2 model. RCP2.6, RCP4.5, and RCP8.5 refer to stabilization without overshoot pathway of 2.6 W/m^2, 4.5 W/m^2, and 8.5 W/m^2, respectively, at stabilization above 2100 (Hijioka et al., 2008).

2.3. Methods

2.3.1. Artificial neural network model

An artificial neural network is a machine learning approach well suited for handling nonlinear problems. It is suitable for solving problems of non-deterministic reasoning with complicated causality and it features an adaptive ability and fault tolerance (Hu et al., 2001). An Artificial Neural Network (ANN) is an effective method of spatial interpolation to downscale GCM. Results from Snell et al. (2000) showed that the ANN approach is superior both in terms of predictive accuracy and model encompassing. Numerous studies used an ANN to downscale GCM data and achieved good results. Chadwick et al. (2010, 2011) used an ANN approach to downscale temperature and rainfall in Europe. Norton et al. (2011) used a statistical model based on a nonlinear ANN to downscale daily extreme precipitation events from general circulation models for future projections in Oahu, Hawaii. Trigo and Palutikof (2001) developed linear and nonlinear downscaling transfer functions based on an ANN to downscale monthly precipitation in the Iberian Peninsula. Abdellatif et al. (2013) used a novel technique for downscaling daily rainfall based on an ANN to downscale rainfall. This research demonstrates that an ANN is an effective method to perform climate downscale. There are many types of neural network models. This study used the widely used back propagation neural network and the output of the model is:

$$y(t) = f\left[\sum_{j=1}^{m} w_j f\left[\sum_{i=1}^{n} v_{ij} x_i(t) + \theta_j\right] + \theta_0\right] \quad (1)$$

where $y(t)$ is the forecast amount of the model output at time t; $f(x)$ is the transfer function,; w_j is the weight coefficient connecting the hidden layer and the output layer; $x_i(t)$ is the model input of the i-th climate factor value at time t; v_{ij} is the weight coefficient connecting the hidden layer and the input layer; n is the dimension of the input layer; m is the dimension of the hidden layer; θ_j is the threshold of the hidden layer; θ_0 is the threshold of the output layer.

In this paper, the observation data, and GCM data from 1961 to 2000 were used as training samples (the coefficient of determination R^2 was between 0.56 and 0.91). Then examined model by the observation data, and GCMs data from 2001 to 2005 (the coefficient of determination R^2 was between 0.53 and 0.90). The model simulation results were satisfactory and were therefore used in the subsequent analysis. Finally, the 2020–2049 GCM data were simulated to obtain the predicted 2020–2049 climate data.

2.3.2. Calculation methods of ET_0 and ET_c

The Penman–Monteith equation was used to calculate ET_0; this equation is based on the principle of energy balance and aerodynamics and was recommended by the FAO in 1998 (Allen et al., 1998). The method has a sound theoretical basis, high accuracy, and is widely used. The Penman–Monteith equation is as follows (Allen et al., 1998):

$$ET_0 = \frac{0.408\Delta(R_n - G) + \gamma\frac{900}{T+273}u_2(e_s - e_a)}{\Delta + \gamma(1 + 0.34u_2)} \quad (2)$$

where ET_0 is the potential evapotranspiration rate, mm d^{-1}; T is the temperature at a height of 2 m, °C; G is the soil heat flux density, MJ m^{-2} day^{-1}; u_2 is the wind speed at a height of 2 m, m s^{-1}; e_s is the saturated water vapor pressure, KPa; e_a is the actual water vapor pressure, KPa; Δ is the slope of the saturation vapor pressure curve, KPa °C^{-1}; γ is the psychrometric constant, KPa °C^{-1}; and R_n is the net radiation, MJ m^{-2} day^{-1}.

The crop coefficient method used to calculate the evapotranspiration is a simple and practical approach that can be used for irrigation system design and irrigation management. The equation (Allen et al., 1998) is as follows:

$$ET_c = K_c \times ET_0 \quad (3)$$

where ET_c is the daily evapotranspiration of the crop, mm d^{-1}; K_c is the crop coefficient, dimensionless.

In this study, five crops are evaluated: apple, jujube, maize, potato, and soybean; the planting areas of these crops accounted for 80.55% of the total planting area in the LPNS.

3. Results

3.1. Prediction of climatic factors under future climate change scenarios

This paper analyzed the spatial and temporal evolution processes and the characteristics of five meteorological parameters (temperature (T), relative humidity (RH), wind speed (WS), effective precipitation (Pe), and sunshine duration (SD)) from ten meteorological stations within the study area under future climate change scenarios. As observed from the spatial distribution of these meteorological factors, the results showed that T, RH, and Pe were higher in the southern region than in the northern region, while SD, and WS exhibited the opposite trend. In addition, the distributions of the meteorological factors in each of the scenarios were different (Fig. 2).

As observed from the temporal evolution of the factors, T had an upward trend in all scenarios at each station and showed a significant

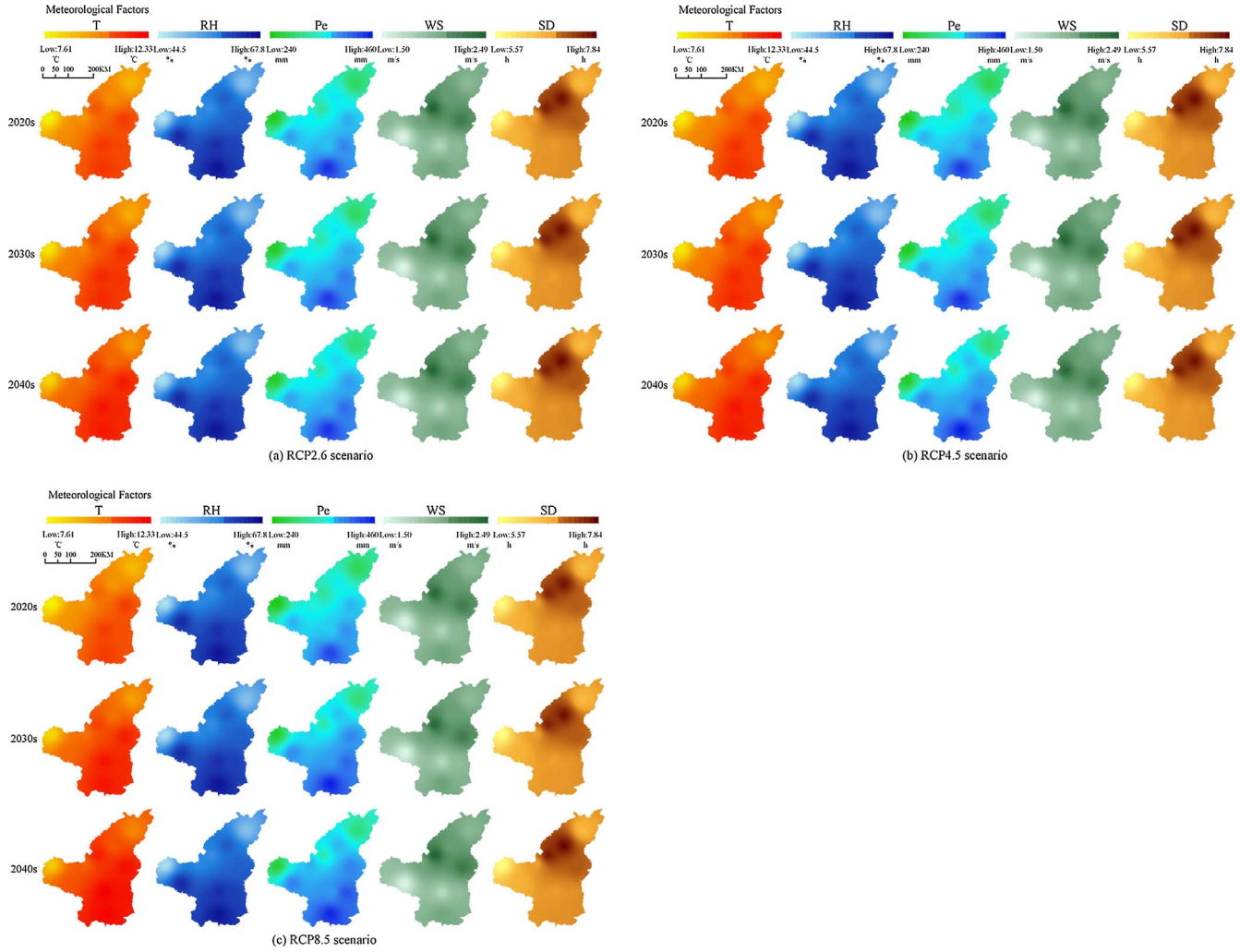

Fig. 2. Spatial and temporal evolution of the main meteorological factors during 2020–2049; (a) RCP2.6 scenario, (b) RCP4.5 scenario, (c) RCP8.5 scenario..

upward trend ($P < 0.05$) in all regions in the RCP8.5 scenario. In the RCP8.5 scenario, the increase in the T was highest at the Hengshan station and the value of the Mann–Kendall (MK) trend test was 3.78 ($P < 0.05$). During the same time, the RH showed an upward trend in all regions for all scenarios and showed a significant upward trend ($P < 0.05$) in the southern region in the RCP4.5 and RCP8.5 scenarios. In the RCP8.5 scenario, the increase in the RH was highest at the Luochuan station and the value of the MK trend test was 3.10 ($P < 0.05$). Pe exhibited an upward trend in all regions in all scenarios with a significant upward trend ($P < 0.05$) in the southern region in the RCP4.5 and RCP8.5 scenarios. The increase in the Pe was highest at the Yanchang Station in the RCP4.5 scenario and the value of the MK trend test was 3.57 ($P < 0.05$). The WS showed a decreasing trend in the southern region in all scenarios. The decrease of the WS was highest at the Yanan station in RCP8.5 and the value of the MK trend test was −3.39 ($P < 0.05$). The SD had no significant trend at any station in all scenarios.

3.2. Crop evapotranspiration under future climate change scenarios

The results showed that the ET was the highest for maize at each station and for each decade in all scenarios, followed by apple, jujube, soybean, and potato (Fig. 3). In all scenarios, the ET of the main crops showed a decreasing but non-significant trend. The decreasing trend of the ET for apple, jujube, maize, and potato during the growing season was higher in the RCP4.5 scenario than in the RCP2.6 and RCP8.5 scenarios. The annual rate of ET change was −0.11 mm/year for apple, −0.16 mm/year for jujube, −0.19 mm/year for maize, and −0.05 mm/year for potato. The decreasing trend of the ET for soybean was highest in the RCP2.6 (−0.05 mm/year) scenario, followed by the RCP4.5 (−0.03 mm/year) and the RCP8.5 (−0.03 mm/year) scenarios. The spatial distributions of the ET for the main crops were similar in all scenarios; the ET was higher in the northern region and lower in the southern and western regions. The ET of maize reached a maximum of 811 mm at the Hengshan station in the RCP4.5 scenario in the 2030s. The ET of potato reached a minimum of 395 mm at the Luochuan station in the RCP8.5 scenario in the 2030s.

3.3. Analysis of supply and demand of water resources for planting under future climate change scenarios

This paper analyzed the evolution of total ET of the crops, Pe in growing period, and irrigation water requirement in different future climate change scenarios. As shown in Fig. 4, the results showed that the annual total ET of the crops in the study area was 5.11×10^9 m^3/year during 2010–2014. In the RCP2.6, RCP4.5, and RCP8.5 scenarios, the annual total ET of the crops during 2040–2049 was 4.75×10^9 m^3/year, 4.73×10^9 m^3/year, and 4.72×10^9 m^3/year, respectively. In the RCP2.6, RCP4.5, and RCP8.5 scenarios, the annual total ET of the crops exhibited a decreasing, non-significant trend and the slopes were -0.06×10^6 m^3/year, -0.13×10^6 m^3/year, and -0.03×10^6 m^3/year, respectively. The decrease in the total ET of the crops was highest

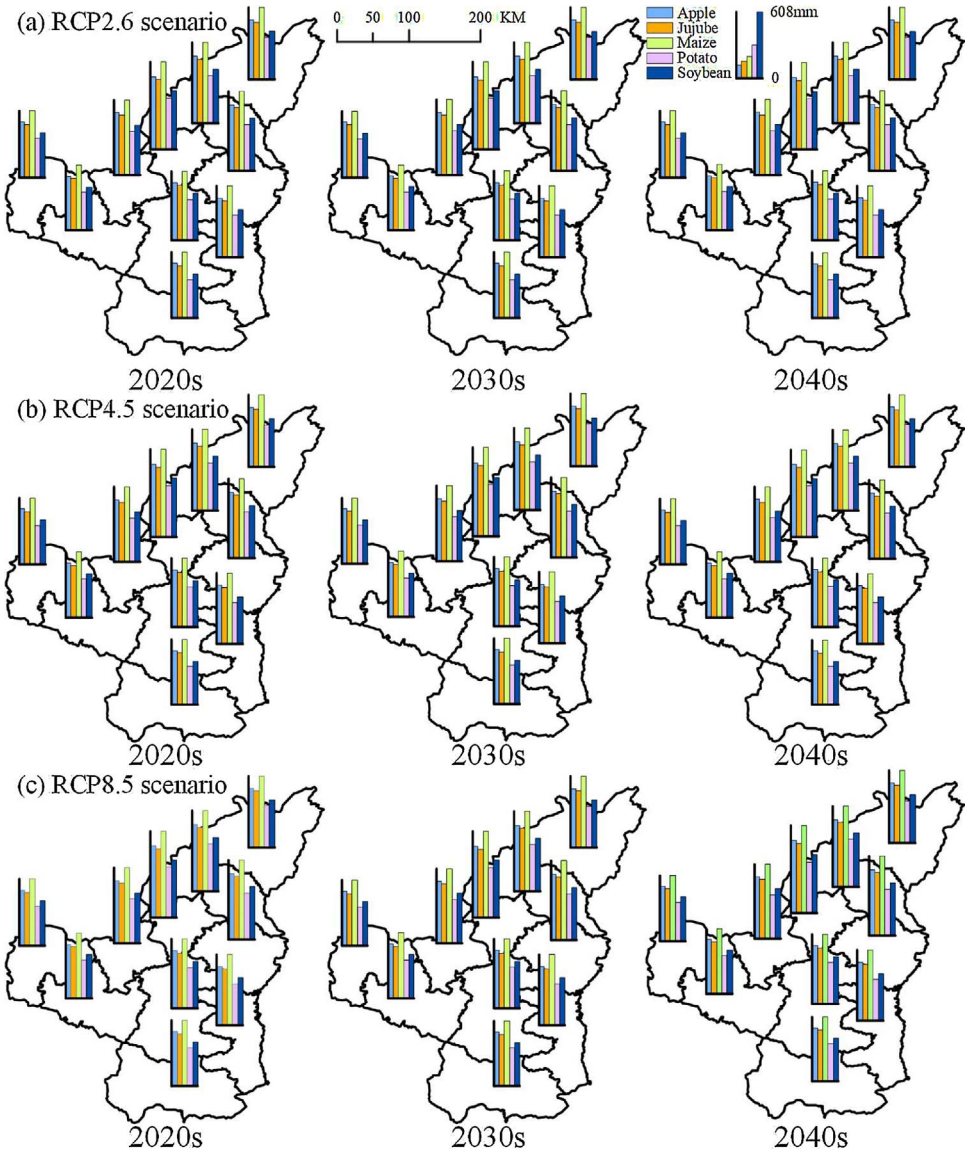

Fig. 3. Spatial and temporal evolution of the evapotranspiration of the main crops; (a) RCP2.6 scenario, (b) RCP4.5 scenario, (c) RCP8.5 scenario.

in the RCP4.5 scenario. At the Suide station, the total ET of the crops exhibited the largest decrease in the RCP8.5 scenario and the average annual descent slope was -0.67×10^6 m^3/year. The total ET of the crops reached a maximum of 1.14×10^9 m^3/year in 2047 and a minimum of 1.04×10^9 m^3/year in 2032. The total ET of the crops in the central and northern regions was lower during 2010–2014 than under the future climate change scenarios and the results for the other regions was the opposite. The total ET of the crops was higher in the eastern region than in the western region in all scenarios.

The annual total Pe in the study area was 3.27×10^9 m^3/year during 2010–2014. In the RCP2.6, RCP4.5, and RCP8.5 scenarios, the annual total Pe during 2040–2049 was 3.46×10^9 m^3/year, 3.53×10^9 m^3/year, and 3.58×10^9 m^3/year, respectively. In the RCP2.6 scenario, the annual total Pe showed an increasing, non-significant trend and the slopes were 0.92×10^6 m^3/year, and 1.1×10^6 m^3/year, respectively. At the Suide station, the total Pe exhibited the largest decrease in the RCP8.5 scenario; the average annual descent slope was 2.47×10^6 m^3/year and the total Pe reached a maximum of 0.752×10^9 m^3/year in 2048 and a minimum of 0.657×10^9 m^3/year in 2023. The total Pe was higher in the western, and northern regions during 2010–2014 than under the future climate change scenarios and the results for the other regions were the opposite. The total Pe was higher in the eastern region than in the western region in all scenarios.

The annual total irrigation water requirements in the study area were 1.84×10^9 m^3/year during 2010–2014. In the RCP2.6, RCP4.5, and RCP8.5 scenarios, the annual total irrigation water requirements during 2040–2049 were 1.29×10^9 m^3/year, 1.20×10^9 m^3/year, and 1.09×10^9 m^3/year, respectively. In the RCP2.6 scenario, the annual total irrigation water requirements showed an increasing, non-significant trend and the slope was -3.98×10^6 m^3/year. In the RCP4.5 and RCP8.5 scenarios, the slopes were -10.1×10^6 m^3/year, and -11.1×10^6 m^3/year, respectively. At the Suide station, the total irrigation water requirements exhibited the largest increase in the RCP8.5 scenario and the average annual descent slope was -2.78×10^6 m^3/year. The total irrigation water requirements reached a maximum of 0.462×10^9 m^3/year in 2021 and a minimum of 0.314×10^9 m^3/year in 2023. In the northern region, the total irrigation water requirements were lower during 2010–2014 than under the future climate change scenario and the results for the other regions were the opposite. The total irrigation water requirements were higher in the northern region than in the southern region in all scenarios.

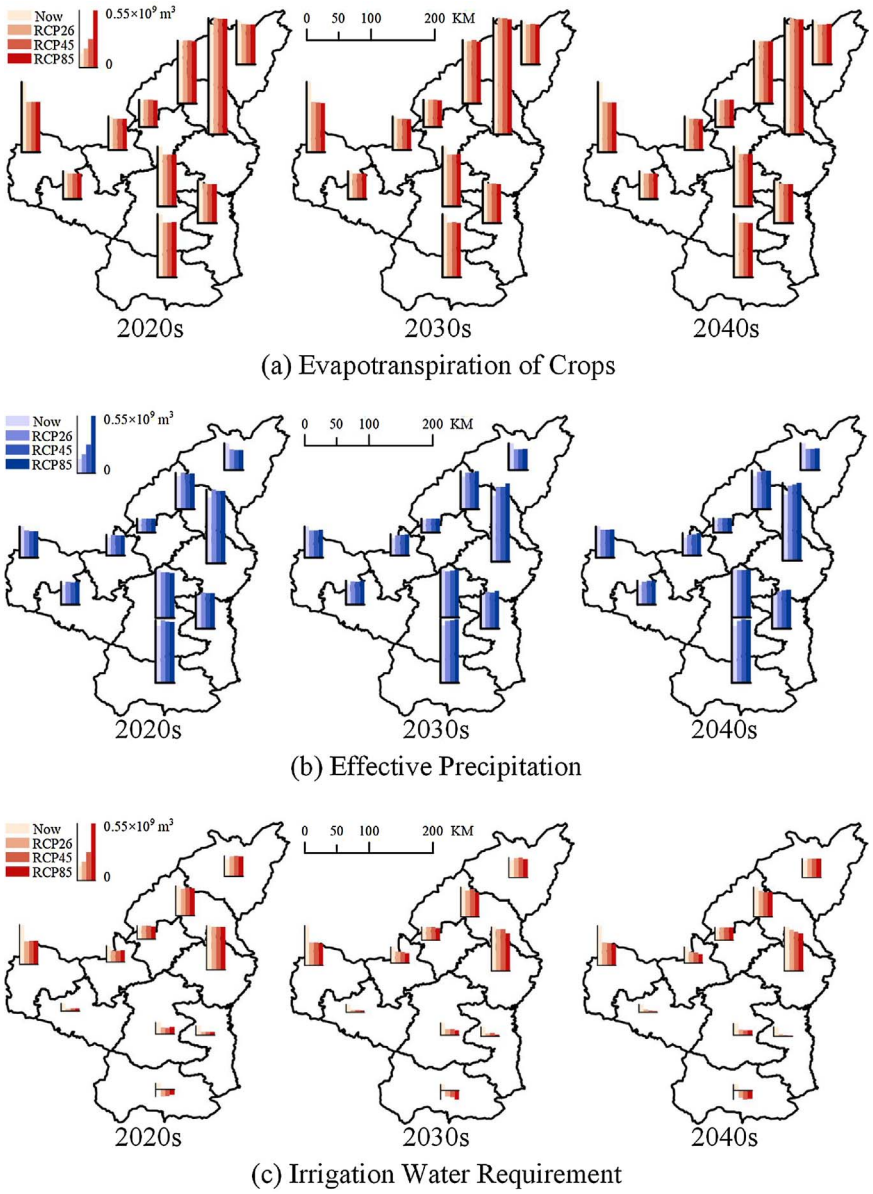

Fig. 4. Spatial and temporal evolution of (a) total evapotranspiration of crops, (b) effective precipitation, and (c) irrigation water requirements.

4. Discussion

4.1. Future climate features in the LPNS

Agricultural production systems are very sensitive to variations in climatic factors. Research on the future spatial and temporal evolution of climatic factors and ET can provide reference information for the management of agricultural water resources and help guide responses to climate change. The Loess Plateau of northern Shaanxi is a water deficient and ecologically fragile area and in recent years, research on the characteristics of climate change in northern Shaanxi has become the focus of many scholars.

As shown in Fig. 5, in the RCP2.6, RCP4.5, and RCP8.5 scenarios, the range of the annual T in the study area was 9.45–11.37 °C, 9.26–11.17 °C, and 9.51–11.48 °C, respectively and the slopes of the annual T were 0.0367 °C/year, 0.0229 °C/year, and 0.0526 °C/year, respectively. In the RCP2.6, RCP4.5, and RCP8.5 scenarios, the range of the annual RH was 56.71–59.23%, 56.96–59.33%, and 57.56–60.16%, respectively and the slopes were 0.0223%/year, 0.0527%/year, and 0.0491%/year, respectively. In the RCP2.6, RCP4.5, and RCP8.5 scenarios, the range of the annual Pe was 349–384 mm, 343–385 mm, and 341–401 mm, respectively and the slopes were 0.3612 mm/year, 0.9533 mm/year, and 1.1369 mm/year, respectively. In the RCP2.6, RCP4.5, and RCP8.5 scenarios, the range of the annual WS was 1.91–2.02 m/s, 1.92–2.01 m/s, and 1.91–2.00 m/s, respectively and the slopes were 0.0001 m/s·year, −0.001 m/s·year, and −0.0002% m/s·year, respectively. In the RCP2.6, RCP4.5, and RCP8.5 scenarios, the ranges of the annual SD were 6.78–6.93 h, 6.76–6.94 h, and 6.76–6.92 h, respectively and the slopes were 0.0011 h/year, −0.001 h/year, and 0.0008 h/year.

The results of this study were consistent with the results of Zhao et al. (2008) and Zhao et al., 2013, the T of the LPNS was on the rise under future climate change scenarios. The RH showed an upward trend in all regions in all scenarios and a significant upward trend ($P < 0.05$) in the southern regions in the RCP4.5 and RCP8.5 scenarios. The Pe was higher in the south than in the north and this is also consistent with the results of Zhao et al. (2008). The Pe showed an upward trend in all scenarios, which is consistent with the results reported by Cao et al. (2010). In the RCP8.5 scenario, there was a significant upward trend ($P < 0.05$) in the southern region. The WS and SD had no significant trends in any scenarios.

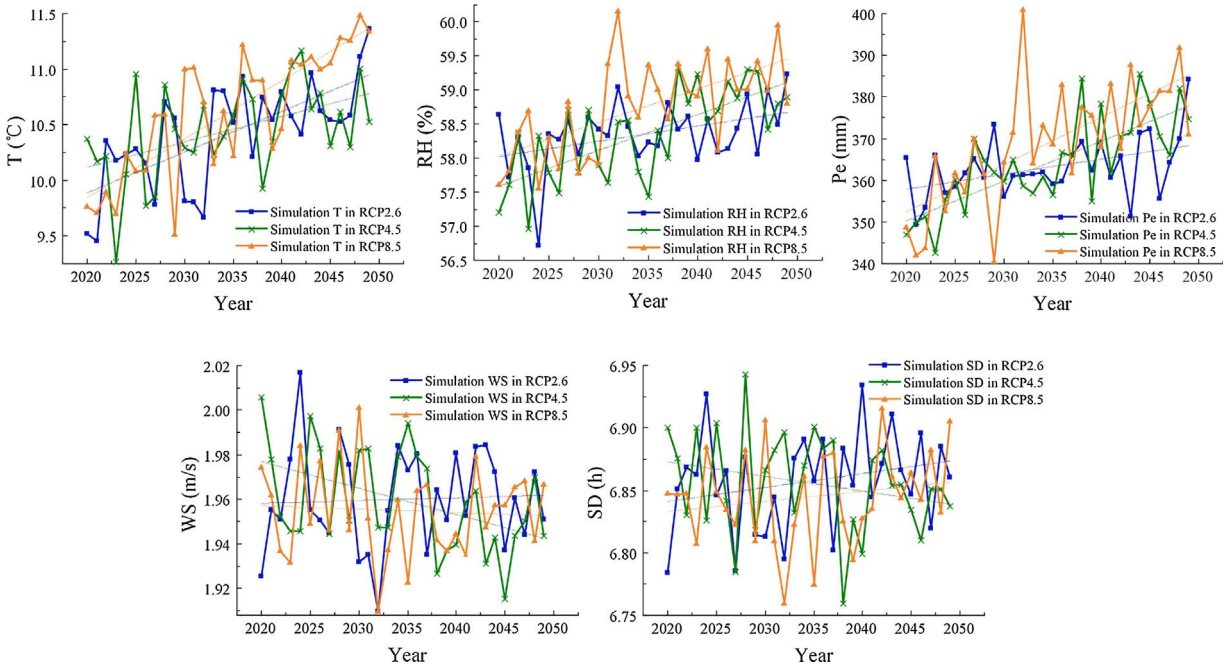

Fig. 5. Temporal evolution of meteorological factors.

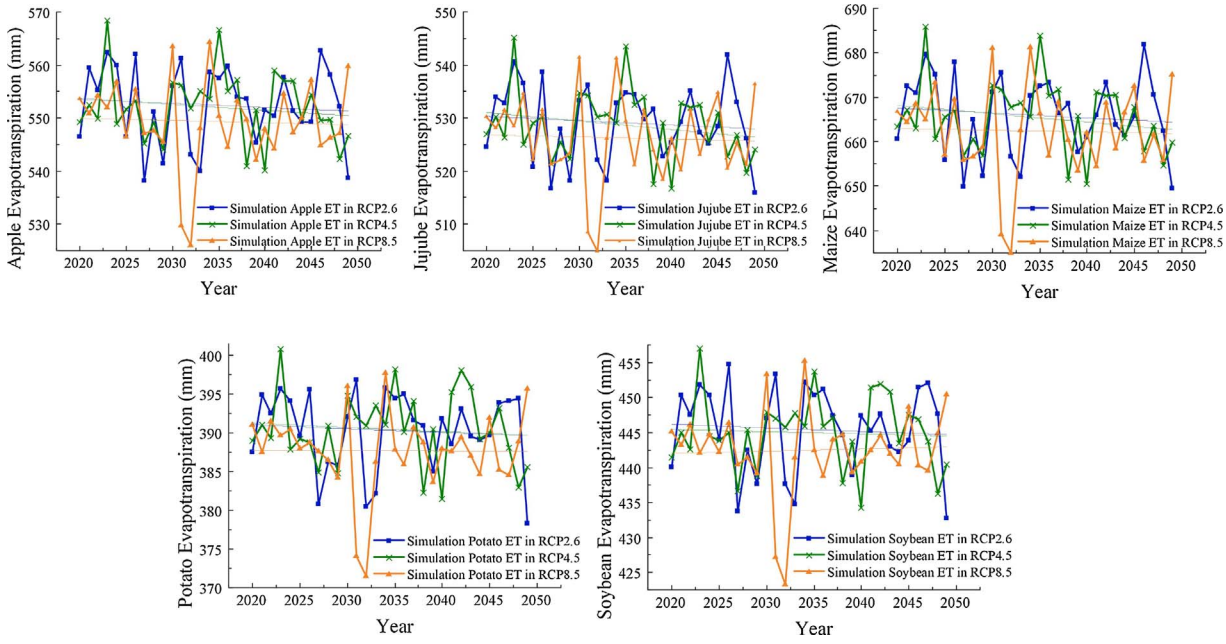
Apple Evapotranspiration (mm)
Simulation Apple ET in RCP2.6
Simulation Apple ET in RCP4.5
Simulation Apple ET in RCP8.5
Jujube Evapotranspiration (mm)
Simulation Jujube ET in RCP2.6
Simulation Jujube ET in RCP4.5
Simulation Jujube ET in RCP8.5
Maize Evapotranspiration (mm)
Simulation Maize ET in RCP2.6
Simulation Maize ET in RCP4.5
Simulation Maize ET in RCP8.5
Potato Evapotranspiration (mm)
Simulation Potato ET in RCP2.6
Simulation Potato ET in RCP4.5
Simulation Potato ET in RCP8.5
Soybean Evapotranspiration (mm)
Simulation Soybean ET in RCP2.6
Simulation Soybean ET in RCP4.5
Simulation Soybean ET in RCP8.5
Year

Fig. 6. Temporal evolution of the evapotranspiration of the main crops.

4.2. Impact of climate change on crop evapotranspiration

Agriculture is seriously affected by climate change. A rise in temperatures will increase crop water requirement, while a reduction in crop yields will be resulted when temperatures constrain the crop development (Allen et al., 1998). To adapt agricultural systems to a changing climate, it is important to know how climate change affects the ET of crops (Sun et al., 2013). Milano et al. (2013) defined the current pressures on water resources and evaluated future changes in water allocation in the medium term under different climatic and water use scenarios in the Ebro catchment. In 2050, water resources were projected to decrease during spring and summer, leading to growing competition among users and severe water shortages for irrigated agriculture in the Ebro catchment. Guo and Shen (2016) predicted potential future climate trends based on the Coupled Model Intercomparison Project Phase 5 (CMIP5) simulations in the arid region of northwestern China. In their study, the annual runoff was predicted to be equivalent to or less than the increased irrigation water requirements in this region over the next 60 years. In addition, the differences between the water supply and demand would result in more severe water shortages in the future.

In the LPNS, the ET of the main crops showed a decreasing, non-significant trend. In the RCP2.6, RCP4.5, and RCP8.5 scenarios, the ranges of the annual ET for apple were 538–563 mm, 540–568 mm, and 526–564 mm, respectively and the slopes were −0.076 mm/year, −0.113 mm/year, and −0.043 mm/year, respectively. In the RCP2.6, RCP4.5, and RCP8.5 scenarios, the ranges of the annual ET for jujube were 516–542 mm, 517–546 mm, and 505–541 mm, respectively and

the slopes were −0.082 mm/year, −0.160 mm/year, and −0.039 mm/year, respectively. In the RCP2.6, RCP4.5, and RCP8.5 scenarios, the ranges of the annual ET for maize were 649–682 mm, 650–686 mm, and 635–681 mm, respectively and the slopes were −0.109 mm/year, −0.189 mm/year, and −0.038 mm/year, respectively. In the RCP2.6, RCP4.5, and RCP8.5 scenarios, the ranges of the annual ET for potato were 378–397 mm, 381–401 mm, and 372–398 mm, respectively and the slopes were −0.048 mm/year, −0.525 mm/year, and −0.002 mm/year, respectively. In the RCP2.6, RCP4.5, and RCP8.5 scenarios, the ranges of the annual ET for soybean were 378–397 mm, 381–401 mm, and 372–398 mm, respectively and the slopes were −0.051 mm/year, −0.034 mm/year, and 0.031 mm/year, respectively (Fig. 6).

Although there were negative effects of the warmer weather on the crop water consumption due to shorter growth periods, lowered stomatal conductance, as well as extreme weather including droughts and floods, the relevant adaptation countermeasures have offset the negative conditions of crop water consumption over the past 30 years (Mo et al., 2013).

Although the annual ET_0 was declining or had no significant trend, the ET of the crops exhibited an upward trend, as was shown in the results of Zhang et al. (2011). As shown in Fig. 6, the ET of the main crops showed a decreasing, non-significant trend. It is possible that the RH had increased. An increase in the RH will directly affect the transpiration of a plant's stomata. At the same temperature, the higher the RH of the atmosphere, the bigger the vapor pressure is; the lower the vapor pressure difference between plant, and atmosphere, the more difficult it is for the water vapor to diffuse outward from the stomata and the lower the transpiration will be (Sun et al., 2017).

In the RCP2.6 scenario, the increase in the total Pe and the decrease in the total ET of the crops resulted in a slight downward trend in the irrigation water requirements. In the RCP4.5, and RCP8.5 scenarios, the increase in the total Pe and the decrease in the total ET of the crops resulted in a significant downward trend ($P < 0.05$) in the irrigation water requirements (Fig. 7).

The level of sustainable use of the water resources was quantitatively evaluated in the LPNS in an earlier study (Liu and Song, 2008). The result showed that the capacity to sustain the water resources of the LPNS showed an upward trend from 1996 to 2005. This capacity was between the low and middle stages, which has potential for improvement.

The study area will become warmer and more humid in the future. Administrators can appropriately reduce the irrigation water and focus on the water demand based on ecological principles. The redistribution of water for crops, the adjustment of irrigated and rainfed lands, and the impact of climate change on total crop yields will be moderate. Despite larger impacts of climate change on the water balance in northern China, the impacts on total crop production will be moderate if farmers will be able to reallocate water among crops and adjust the irrigated and rainfed lands (Wang et al., 2013). An increase in the demand for agricultural water under climate change brought on by increasing temperatures will place additional stresses on the water system; therefore, some water users will experience a decrease in the reliability of the water supply (Joyce et al., 2011).

A statistical downscaling approach can provide seemingly credible future climate simulation results but a large amount of uncertainty remains with regard to the application. Among the various sources of uncertainty, the use of the GCMs as the main input source for the statistical downscaling plays a dominant role (Giorgi and Mearns, 2002). The uncertainty of the statistical downscaling method has two aspects. One is related to the choice of the forecasting factors. The choice in the selection method and the strategy, the use of different grid areas for the forecasting factors, and the use of different seasons have a great influence on the forecasting results (Chen et al., 2010). The second aspect is related to the statistical downscaling method itself. The mathematical models are different for different statistical downscaling methods; therefore, the ability to simulate the mean, the extremes, the seasonal distribution, the interannual fluctuation, and the spatiotemporal correlation differs for the various models. In addition, the applicability of different models in different regions varies and all these factors will result in a certain level of uncertainty.

5. Conclusion

In the RCP2.6, RCP4.5, and RCP8.5 scenarios, the T, Pe, and RH increased, the WS decreased slightly, and the trend of the SD was not clear. In the RCP8.5 scenario, the slope of the T reached the maximum of 9.66 °C (2010–2014 average) and decreased to 11.11 °C (2040–2049 average), representing a decrease in 15.01%. In the RCP8.5 scenario, the slope of the Pe reached the maximum of 350 mm (2010–2014 average) and increased to 378 mm (2040–2049 average), representing an increase of 8.00%.

The irrigation water requirements of the main crops exhibited a downward trend in the LPNS under future climate change scenarios. The decreasing trend of the irrigation water requirements were highest in the RCP8.5 scenario (−0.90%), followed by the RCP4.5 (−0.77%) and RCP2.6 (−0.30%) scenarios.

Based on the impact of the changes in the ET and the Pe of future crops, the irrigation water requirements of the agricultural industry showed a downward trend from 1.84×10^9 m^3/year (2010–2014 average) to 1.29×10^9 m^3/year (2040–2049 average) in the RCP2.6 scenario. In the RCP4.5 and RCP8.5 scenarios, the irrigation water requirements of the agricultural industry showed a significant downward trend ($P < 0.05$) from 1.84×10^9 m^3/year (2010–2014 average) to 1.20×10^9 m^3/year (2040–2049 average) and to 1.15×10^9 m^3/year (2040–2049 average), respectively.

Acknowledgements

This work was jointly supported by the National Key Research and Development Program of China (2016YFC0400201), the National Natural Science Foundation of China (51409218), the Natural Science

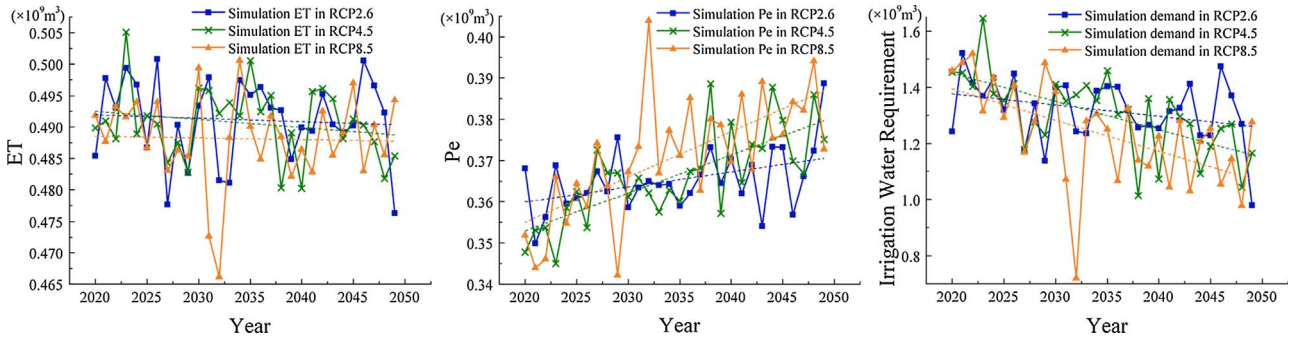

Fig. 7. Temporal evolution of evapotranspiration, effective precipitation, and irrigation water requirements.

Basic Research Plan, Shaanxi Province of China (2016JQ5092), Science and Technology Integrated Innovation Project, Shaanxi Province of China (2016TZC-N-14-1).

References

Abdellatif, M., Atherton, W., Alkhaddar, R., 2013. A hybrid generalised linear and Levenberg–Marquardt artificial neural network approach for downscaling future rainfall in North Western England. Hydrol. Res. 44 (6), 1084–1101.

Allen, R.G., Pereira, L.S., Raes, D., Smith, M., 1998. Crop Evapotranspiration-Guidelines for Computing Crop Water Requirements-FAO Irrigation and Drainage Paper 56. FAO, pp. 56.

Bussel, L.G.J.V., Ewert, F., Zhao, G., Hoffmann, H., Enders, A., Wallach, D., et al., 2016. Spatial sampling of weather data for regional crop yield simulations. Agric. For. Meteorol. 220, 101–115.

CCCma, 2017, http://www.ec.gc.ca/ccmac-cccma/.

Cao, Y., Zhang, G.H., Luo, R.T., 2010. Response of runoff and sediment discharge to global climate change in Jinghe River Basin. Sci. Soil Water Conserv. 8 (2), 30–35.

Chadwick, R., Coppola, E., Giorgi, F., 2010. Downscaling of GCM parameter outputs to RCM spatial scale using an artificial neural network. Temp. Field 12.

Chadwick, R., Coppola, E., Giorgi, F., 2011. An artificial neural network technique for downscaling GCM outputs to RCM spatial scale. Nonlinear Process. Geophys. 18 (6), 1013–1028.

Chen, S.T., Yu, P.S., Tang, Y.H., 2010. Statistical downscaling of daily precipitation using support vector machines and multivariate analysis. J. Hydrol. 385 (1–4), 13–22.

CMA, 2015. China Meteorological Administration. http://cdc.cma.gov.cn.

Fischer, G., Tubiello, F.N., Velthuizen, H.V., Wiberg, D.A., 2007. Climate change impacts on irrigation water requirements: effects of mitigation, 1990–2080. Technol. Forecast. Soc. Change 74 (7), 1083–1107.

Gao, G., Chen, D., Ren, G., Chen, Y., Liao, Y., 2006. Spatial and temporal variations and controlling factors of potential et in China: 1956–2000. J. Geogr. Sci. 16 (1), 3–12.

Giorgi, F., Mearns, L.O., 2002. Calculation of average, uncertainty range, and reliability of regional climate changes from AOGCM simulations via the Reliability Ensemble Averaging (REA) method. J. Clim. 15 (10), 1141–1158.

Groisman, P.Y., Karl, T.R., Easterling, D.R., Knight, R.W., Jamason, P.F., Hennessy, K.J., et al., 1999. Changes in the probability of heavy precipitation: important indicators of climatic change. Clim. Change 42 (1), 243–283.

Guo, Y., Shen, Y., 2016. Agricultural water supply/demand changes under projected future climate change in the arid region of northwestern China. J. Hydrol. 540, 257–273.

Hijioka, Y., Matsuoka, Y., Nishimoto, H., Masui, T., Kainuma, M., 2008. Global ghg emission scenarios under ghg concentration stabilization targets. J. Glob. Environ. Eng. 13, 97–108.

Hu, J.L., Zhang, L.P., Yu, R.C., 2001. The study on applying neural network models to prediction of summer precipitation in Hubei province. Acta Meteorol. Sin. 59 (6), 776–783.

Huntington, T.G., 2006. Evidence for intensification of the global water cycle: review and synthesis. J. Hydrol. 319 (1–4), 83–95.

Joyce, B.A., Mehta, V.K., Purkey, D.R., Dale, L.L., Hanemann, M., 2011. Modifying agricultural water management to adapt to climate change in California's central valley. Clim. Change 109 (1), 299–316.

Li, C., Wu, P.T., Li, X.L., Zhou, T.W., Sun, S.K., Wang, Y.B., et al., 2017. Spatial and temporal evolution of climatic factors and its impacts on potential evapotranspiration in loess plateau of Northern Shaanxi, China. Sci. Total Environ. 589, 165–172.

Liu, D.D., Song, S.B., 2008. Assessment of sustainable utilization of water resources of North Shaanxi. Agric. Res. Arid Areas 26 (4), 254–259.

Luo, Q., Bange, M., Clancy, L., 2014. Cotton crop phenology in a new temperature regime. Ecol. Modell. 285 (1789), 22–29.

Menzel, L., Bürger, G., 2002. Climate change scenarios and runoff response in the mulde catchment (Southern Elbe, Germany). J. Hydrol. 267 (1–2), 53–64.

Milano, M., Ruelland, D., Dezetter, A., Fabre, J., Ardoin-Bardin, S., Servat, E., 2013. Modeling the current and future capacity of water resources to meet water demands in the Ebro basin. J. Hydrol. 500 (11), 114–126.

Mo, X., Guo, R., Liu, S., Lin, Z., Shi, H., 2013. Impacts of climate change on crop evapotranspiration with ensemble GCM projections in the north China plain. Clim. Change 120 (1), 299–312.

Moriondo, M., Bindi, M., 2006. Comparison of temperatures simulated by gcms, rcms and statistical downscaling: potential application in studies of future crop development. Clim. Res. 30 (2), 149–160.

Norton, C.W., Chu, P.S., Schroeder, T.A., 2011. Projecting changes in future heavy rainfall events for Oahu, Hawaii: a statistical downscaling approach. J. Geophys. Res. 116 (D17), 1161–1166.

Shabani, F., Kotey, B., 2016. Future distribution of cotton and wheat in Australia under potential climate change. J. Agric. Sci. 154 (2), 175–185.

Silva, C.S.D., Weatherhead, E.K., Knox, J.W., Rodriguez-Diaz, J.A., 2007. Predicting the impacts of climate change—a case study of paddy irrigation water requirements in Sri Lanka. Agric. Water Manage. 93 (1–2), 19–29.

Snell, S.E., Gopal, S., Kaufmann, R.K., 2000. Spatial interpolation of surface air temperatures using artificial neural networks: evaluating their use for downscaling GCMs. J. Clim. 13 (5), 886–895.

Sun, S., Wu, P., Wang, Y., Zhao, X., Liu, J., Zhang, X., 2013. The impacts of interannual climate variability and agricultural inputs on water footprint of crop production in an irrigation district of China. Sci. Total Environ. 444 (2), 498–507.

Sun, Z., Jia, S.F., Lv, A.F., Zhu, W.B., Gao, Y.C., 2015. Assessment on precision of temperature simulated by the IPCC AR5 GCMs in China, 1996–2005. Progress Geogr. 34 (10), 1229–1240.

Sun, S.K., Wang, Y.B., Liu, J., Cai, H.J., Wu, P.T., Xu, L.J., Geng, Q.L., 2016a. Sustainability assessment of regional water resources under the DPSIR framework. J. Hydrol. 532, 140–148.

Sun, S.K., Wang, Y.B., Engel, B.A., Wu, P.T., 2016b. Effects of virtual water flow on regional water resource stress: a case study of grain in China. Sci. Total Environ. 550, 871–879.

Sun, S.K., Zhang, C.F., Li, X.L., Zhou, T.W., Wang, Y.B., Wang, P.T., Cai, H.J., 2017. Sensitivity of crop water productivity to the variation of agricultural and climatic factors: a study of Hetao irrigation district, China. J. Clean. Prod. 142, 2562–2569.

Tao, F., Yokozawa, M., Hayashi, Y., Lin, E., 2003. Future climate change, the agricultural water cycle, and agricultural production in China. Agric. Ecosyst. Environ. 95 (1), 203–215.

Tao, F., Hayashi, Y., Zhao, Z., Sakamoto, T., Yokozawa, M., 2008. Global warming, rice production, and water use in China: developing a probabilistic assessment. Agric. For. Meteorol. 148 (1), 94–110.

Toews, M.W., Allen, D.M., 2009. Evaluating different gcms for predicting spatial recharge in an irrigated arid region. J. Hydrol. 374 (3–4), 265–281.

Trigo, R.M., Palutikof, J.P., 2001. Precipitation scenarios over Iberia: a comparison between direct GCM output and different downscaling techniques. J. Clim. 14 (23), 4422–4446.

Wang, J.X., Huang, J.K., Yan, T.T., 2013. Impacts of climate change on water and agricultural production in ten large river basins in China. J. Integr. Agric. 12 (7), 1267–1278.

Wen, Q.H., Zhang, X., Xu, Y., Wang, B., 2013. Detecting human influence on extreme temperatures in china. Geophys. Res. Lett. 40 (6), 1171–1176.

Wu, L.L., Ren, Z.Y., Zhang, C., 2014. Response of NDVI to temperature and precipitation changes and its lag time in north Shaanxi. Chin. J. Agrometeorology 35 (1), 103–108.

Zhang, Q., Xu, C.Y., Becker, S., Zhang, Z.X., Chen, Y.D., Coulibaly, M., 2009. Trends and abrupt changes of precipitation maxima in the pearl river basin, China. Atmos. Sci. Lett. 10 (2), 132–144.

Zhang, X., Chen, S., Sun, H., Shao, L., Wang, Y., 2011. Changes in evapotranspiration over irrigated winter wheat and maize in north China plain over three decades. Agric. Water Manage. 98 (6), 1097–1104.

Zhao, C.Y., Nan, Z.R., Cheng, G.D., Zhou, S.B., Zhang, Y.Z., 2008. Prediction of the trend of the future climate change in northwestern China by statistical downscaling. J. Lanzhou Univ. (Nat. Sci.) 44 (5), 12–18.

Zhao, C., Li, Z., Liu, W.Z., 2013. Projecting the potential changes of temperature in the Jinghe watershed using downscaling. J. Northwest A & F Univ. (Nat. Sci. Ed.) 41 (6), , 227–234.

Ziegler, A.D., Sheffield, J., Maurer, E.P., Nijssen, B., Wood, E.F., Lettenmaier, D.P., 2003. Detection of intensification in global- and continental-scale hydrological cycles: temporal scale of evaluation. J. Clim. 16 (3), 535–547.